

# High-Field Magnetoelectric and Spin-Phonon Coupling in Multiferroic $(\text{NH}_4)_2[\text{FeCl}_5 \cdot (\text{H}_2\text{O})]$

Kendall D. Hughey, Minseong Lee, Jisoo Nam, Amanda J. Clune, Kenneth R. O'Neal, Wei Tian, Randy S. Fishman, Mykhaylo Ozerov, JunHee Lee, Vivien S. Zapf, and Janice L. Musfeldt\*



Cite This: *Inorg. Chem.* 2022, 61, 3434–3442



Read Online

ACCESS |



Metrics & More

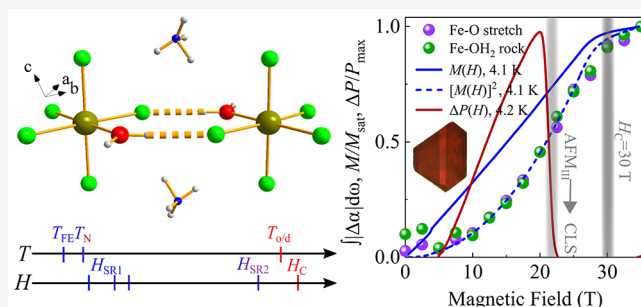


Article Recommendations



Supporting Information

**ABSTRACT:** We combine high field polarization, magneto-infrared spectroscopy, and lattice dynamics calculations with prior magnetization to explore the properties of  $(\text{NH}_4)_2[\text{FeCl}_5 \cdot (\text{H}_2\text{O})]$ —a type II molecular multiferroic in which the mixing between charge, structure, and magnetism is controlled by intermolecular hydrogen and halogen bonds. Electric polarization is sensitive to the series of field-induced spin reorientations, increasing linearly with the field and reaching a maximum before collapsing to zero across the quasi-collinear to collinear-sinusoidal reorientation due to the restoration of inversion symmetry. Magnetoelectric coupling is on the order of 1.2 ps/m for the  $P||c$ ,  $H||c$  configuration between 5 and 25 T at 1.5 K. In this range, the coupling takes place via an orbital hybridization mechanism. Other forms of mixing are active in  $(\text{NH}_4)_2[\text{FeCl}_5 \cdot (\text{H}_2\text{O})]$  as well. Magneto-infrared spectroscopy reveals that all of the vibrational modes below  $600 \text{ cm}^{-1}$  are sensitive to the field-induced transition to the fully saturated magnetic state at 30 T. We analyze these local lattice distortions and use frequency shifts to extract spin-phonon coupling constants for the Fe–O stretch, Fe–OH<sub>2</sub> rock, and NH<sub>4</sub><sup>+</sup> libration. Inspection also reveals subtle symmetry breaking of the ammonium counterions across the ferroelectric transition. The coexistence of such varied mixing processes in a platform with intermolecular hydrogen- and halogen-bonding opens the door to greater understanding of multiferroics and magnetoelectrics governed by through-space interactions.



## INTRODUCTION

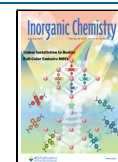
Single phase materials that fully couple ferroelectricity and ferromagnetism have been challenging to realize due to the exacting combination of ultralow symmetries required. While type I multiferroics trigger electric and spin orders independently, type II systems host inversion symmetry breaking magnetic order.<sup>1</sup> The latter is the most effective avenue to robust magnetoelectric coupling. Many materials offer tunable routes to broken spatial inversion and time reversal symmetries,<sup>1–4</sup> although complete (100%) magnetoelectric coupling depends upon inversion symmetry breaking magnetic orders and facile routes for creating electric dipoles. Molecule-based materials offer these opportunities in abundance. They retain many of the same physical characteristics as the oxides while offering lower energy scales, tunable chemical architectures, flexible lattices, and rich phase diagrams.<sup>5–12</sup> This makes molecule-based multiferroics like  $[(\text{CH}_3)_2\text{NH}_2]\text{Mn}(\text{HCOO})_3$ ,  $\text{Cu}(\text{CH}_3)_2\text{SOCl}_2$ , and  $\text{Cu}(\text{pyz})(\text{gly})\text{ClO}_4$  superb platforms for exploring unique states of matter away from equilibrium.<sup>5,13–17</sup> Others including  $\kappa\text{-(BEDT-TTF)}_2\text{Cu}[\text{N}(\text{CN})_2]\text{Cl}$  and  $\text{NiCl}_2\text{--}4\text{SC}(\text{NH}_2)_2$  are wholly molecular in nature with through-space intermolecular interactions that provide both electric and magnetic functionality.<sup>18,19</sup> In this

work, we build upon recent magnetization and neutron scattering on multiferroic  $(\text{NH}_4)_2[\text{FeCl}_5 \cdot (\text{H}_2\text{O})]$ <sup>20–25</sup> with a combination of high field electric polarization, magneto-infrared spectroscopy, and first-principles lattice dynamics calculations. By so doing, we provide a framework for understanding the interplay between charge, structure, and magnetism in this system.

$(\text{NH}_4)_2[\text{FeCl}_5 \cdot (\text{H}_2\text{O})]$  is the multiferroic member of the  $A_2[\text{BX}_5 \cdot (\text{H}_2\text{O})]$  family of erythrosiderites ( $A = \text{K}^+, \text{Rb}^+, \text{NH}_4^+$ ;  $B = \text{Fe}^{3+}, \text{Mn}^{3+}, \text{Co}^{3+}$ ;  $X = \text{Cl}^-, \text{Br}^-, \text{H}_2\text{O}$ ). In this system,  $[\text{FeCl}_5(\text{H}_2\text{O})]^{2-}$  groups are arranged in a herringbone-like pattern along the  $b$  axis (Figure 1a). The overall structure is governed by an extensive network of intermolecular hydrogen and halogen bonding.<sup>20,26–30</sup> Ammonium ( $\text{NH}_4^+$ ) fills the anion pocket and balances charge. This material is magnetically complex with five unique but nearly iso-energetic exchange

Received: October 24, 2021

Published: February 16, 2022



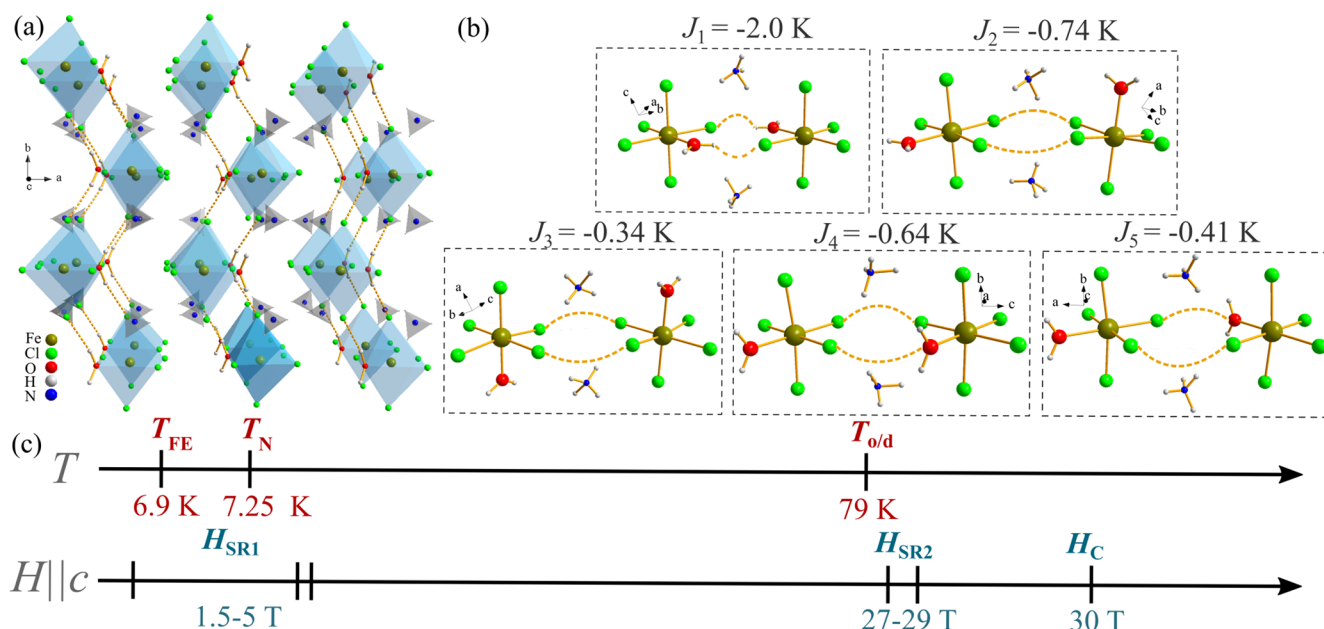


**Figure 1.** (a) Crystal structure of  $(\text{NH}_4)_2[\text{FeCl}_5 \cdot (\text{H}_2\text{O})]$  at room temperature.<sup>20</sup> The primary hydrogen-bonding interactions (arising from  $J_1$ ) yield herringbone-like connectivity. (b) Summary of the five exchange pathways mediated by hydrogen- and halogen-bonding. The strength of each pathway is indicated. These values are determined from fits to the neutron scattering data.<sup>25</sup>  $J_1$  involves purely hydrogen bonds with a  $\text{O} \cdots \text{H} \cdots \text{Cl}$  pathway.  $J_2$  and  $J_3$  have  $\text{Cl} \cdots \text{Cl}$  interactions, and  $J_4$  and  $J_5$  have asymmetric pathways with one  $\text{Cl} \cdots \text{O}$  and one  $\text{Cl} \cdots \text{Cl}$  pathway.<sup>26–29</sup> All of these superexchange pathways arise from intermolecular interactions. Weak interactions between the H centers of the ammonium counterion and the Cl and O ions are also present.<sup>27,28,30</sup> We employ a single  $J$  Hamiltonian, and the negative sign indicates antiferromagnetic interactions. The in-plane anisotropy  $D$  is  $0.17$  K.<sup>25</sup> (c) Summary of temperature- and field-driven transitions.  $T_{o/d}$  is the order/disorder transition.  $T_N$  is the Néel transition, and  $T_{\text{FE}}$  is the ferroelectric transition temperature. Under a magnetic field, there is a series of low field spin reorientations between 1 and 5 T that we refer to as  $H_{\text{SR1}}$ .  $H_{\text{SR2}}$  and  $H_C$  are the high field spin reorientations between 27 and 29 T and saturation field, respectively.

pathways ( $J_{1-5}$ ), all of which are associated with various types of  $\text{OH} \cdots \text{Cl}$  and  $\text{Cl} \cdots \text{Cl}$  interactions (Figure 1b).<sup>7,20,27–30</sup> In other words, it is the intermolecular hydrogen and halogen bonding rather than traditional chemical bonds that create the superexchange pathways.<sup>26</sup> The  $\text{NH}_4^+$  counterions contribute to these through-space interactions as well.  $(\text{NH}_4)_2[\text{FeCl}_5 \cdot (\text{H}_2\text{O})]$  displays a series of temperature-driven transitions (Figure 1c) including an order–disorder transition at  $79$  K;<sup>24</sup> magnetic ordering of the  $S = 5/2$   $\text{Fe}^{3+}$  centers below  $T_N = 7.25$  K that creates a collinear sinusoidal spin wave structure with  $K = (0, 0, 0.23)$ <sup>23</sup> and ferroelectricity below  $T_{\text{FE}} = 6.9$  K that arises due to the development of an incommensurate-cycloidal spin state  $K_1 = (0, 0, 0.23)$  that coexists (and competes) with a commensurate distorted cycloidal phase  $K_2 = (0, 0, 0.25)$ .<sup>23</sup> Modeling of the inelastic neutron scattering reveals that  $J_2$  and  $J_4$  are the sources of frustration and responsible for the cycloidal character of the spin waves.<sup>25</sup> Numerical simulation shows that in-plane magnetic anisotropies as well as geometrical frustration in the exchange interactions stabilize the collinear sinusoidal phase.<sup>31</sup>  $(\text{NH}_4)_2[\text{FeCl}_5 \cdot (\text{H}_2\text{O})]$  is a type II system.<sup>1</sup> Multiferroicity arises from an inverse Dzyaloshinskii–Moriya (spin-current) mechanism in which the spin cycloid breaks inversion symmetry.<sup>4,32</sup> The microscopic nature of the lattice distortion that creates electric polarization is not known at the present time.

Under a magnetic field,  $(\text{NH}_4)_2[\text{FeCl}_5 \cdot (\text{H}_2\text{O})]$  undergoes a series of frustration-induced spin reorientations between 1 and 5 T.<sup>20,21</sup> Several high field spin reorientations take place before the transition to the fully saturated magnetic state at  $H_C = 30$  T as well (Figure 1c).<sup>21</sup> Spin density calculations reveal how intermolecular interactions support magnetic exchange and

how these pathways change across the transition to the fully saturated state.<sup>21</sup> Electric polarization is closely linked to magnetization. In fact, the series of low field spin reorientations triggers polarization flops as well as changes in the elastic response at  $5$  T.<sup>23</sup> Curiously, multiferroicity in the commensurate quasi-collinear state ( $K_3 = 0, 0, 0$ ) above  $5$  T is described by the spin-dependent p–d hybridization model<sup>32–36</sup> rather than an inverse Dzyaloshinskii–Moriya mechanism. Evidence for this mechanistic crossover comes from neutron diffraction measurements,<sup>32</sup> although in this system, the exchange interactions do not follow traditional chemical bonds but instead go between the  $\text{Fe}^{3+}$  centers in such a way as to make use of the  $\text{Cl}^-$  ligands and the  $\text{NH}_4^+$  ions as shown in Figure 1b. Thus, there are two distinct magnetoelectric coupling mechanisms in the same material: (i) inverse Dzyaloshinskii–Moriya between  $0$  and  $5$  T and (ii) p–d hybridization above  $5$  T, rather than a single overarching mechanism. This situation is unexpected and merits investigation. To our knowledge, a field-dependent magnetoelectric coupling mechanism is observed in only one other material,  $\text{Ni}_2\text{Mo}_3\text{O}_8$ .<sup>37</sup> In any case, the noncollinear spin structure and ferroelectric phases are rather fragile—a finding reinforced by potassium substitution studies in  $[(\text{NH}_4)_{1-x}\text{K}_x][\text{FeCl}_5 \cdot (\text{H}_2\text{O})]$ .<sup>38</sup> Magnetoelectric and magnetoelastic coupling at higher fields are wholly unexplored—a process made all the more intriguing by the presence of a field dependent magnetoelectric coupling mechanism.

Inspired by the discovery of complex spin-charge interactions in a purely molecular multiferroic, we combined several techniques that are rarely brought together—high field polarization, magneto-infrared spectroscopy, first-principles

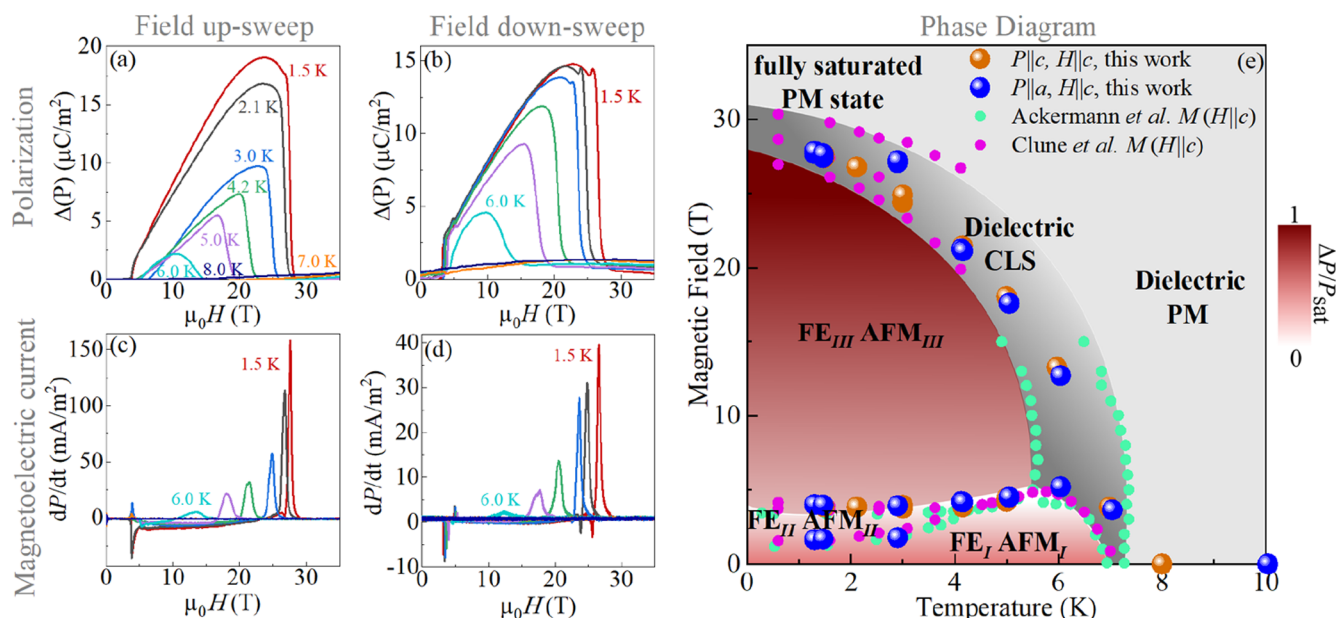


**Figure 2.** (a,b) Change in electric polarization ( $\Delta P$ ) of  $(\text{NH}_4)_2[\text{FeCl}_5 \cdot (\text{H}_2\text{O})]$  as a function of magnetic field (up- and down-sweeps) at various temperatures. This is the  $P||c, H||c$  configuration. Others are given in the Supporting Information. In each case, polarization is measured after poling the sample in an electric field. (c,d) Magneto-electric current  $I = dP/dt$  vs applied field, highlighting changes in  $\Delta P(H)$ . (e)  $H$ – $T$  phase diagram of  $(\text{NH}_4)_2[\text{FeCl}_5 \cdot (\text{H}_2\text{O})]$  derived from the magnetization<sup>21</sup> along with points taken from our magneto-electric current measurements. The latter are indicated as orange ( $P||c, H||c$ ) and blue ( $P||a, H||c$ ) spheres; for both configurations, the up-sweep data were used to construct the phase diagram. Here, FE = ferroelectric, AFM = antiferromagnetic, CLS = collinear sinusoidal, and PM = paramagnetic. A color bar is included to indicate the size of  $\Delta P/P_{\text{sat}}$ . The latter is defined as the field-induced change in polarization divided by the maximum polarization at a given temperature. Polarization emanates from the  $[\text{FeCl}_5(\text{H}_2\text{O})]^{2-}$  framework (and the cycloidal spin state on the  $\text{Fe}^{3+}$  centers), not the  $\text{NH}_4^+$  counterion.

lattice dynamics calculations, and magnetization<sup>21</sup>—to uncover magneto-electric and spin-phonon interactions in  $(\text{NH}_4)_2[\text{FeCl}_5 \cdot (\text{H}_2\text{O})]$ . We demonstrate that this system is indeed a multiferroic with strong magneto-electric coupling and peaks in the magneto-electric current at the significant phase boundaries. We find a maximum  $\Delta P$  of  $19 \mu\text{C}/\text{m}^2$  near 24 T and deterministic control of this quantity between approximately 5 and 25 T due to systematic spin canting. The magneto-electric coupling constant  $\alpha_{\text{me}}$  is on the order of 1.2 ps/m for the  $P||c, H||c$  configuration between 5 and 25 T at 1.5 K. This interaction derives from orbital hybridization. In a dramatic demonstration of how inversion symmetry impacts the properties of a type II multiferroic, polarization plunges to zero across the field-driven quasi-collinear  $\rightarrow$  collinear sinusoidal magnetic orientation transition, and it remains flat across the 30 T magnetic saturation transition due to restoration of the inversion center. At the same time, we show that other forms of cross-coupling—in addition to magneto-electric interactions—are active in  $(\text{NH}_4)_2[\text{FeCl}_5 \cdot (\text{H}_2\text{O})]$ . Magneto-infrared spectroscopy reveals spin-phonon coupling involving the majority of low-frequency modes across the magnetic phase transition. The librational modes involving ammonium and water have the largest amplitude changes, whereas the Fe–O stretch and Fe–OH<sub>2</sub> rock have the most sizable coupling constants. We also employ the magneto-infrared spectra to uncover subtle symmetry breaking of the ammonium counterions across the ferroelectric phase transition. These findings demonstrate how charge, structure, and magnetism mix using only intermolecular hydrogen and halogen bonding to create strongly coupled functionalities in an ultralow symmetry molecular multiferroic.

## RESULTS AND DISCUSSION

**Magneto-electric Coupling Across the Magnetically Driven Transitions.** Figure 2 summarizes the magneto-electric properties of  $(\text{NH}_4)_2[\text{FeCl}_5 \cdot (\text{H}_2\text{O})]$  in the  $P||c, H||c$  configuration. Similar results in other measurement configurations are given in the Supporting Information. Figure 2a,b highlight the change in electric polarization  $\Delta P$  as a function of magnetic field (up and down sweeps) at temperatures both above and below  $T_{\text{FE}} = 6.9$  K. At low fields,  $\Delta P$  is zero, consistent with prior work.<sup>20</sup> This finding indicates that polarization lies primarily within the  $ab$  plane ( $9^\circ$  off of the  $a$  axis) in zero field.<sup>20</sup> A polarization flop to the  $c$  axis is responsible for the sharp rise near 5 T.<sup>20,39</sup> We find that  $\Delta P$  rises above the spin flop transition, increasing almost linearly with field in the ferroelectric state. At the base temperature,  $\Delta P$  reaches a maximum of  $19 \mu\text{C}/\text{m}^2$  near 24 T at 1.5 K, starts to decrease slightly, and then plunges to zero near 27 T. This is consistent with a type II mechanism in which magnetic order breaks inversion symmetry.<sup>1</sup> The overall magnitude of  $\Delta P$  is smaller at 4 K, and the collapse occurs at a significantly lower magnetic field than in the 1.5 K data. The 6 K curve shows modest signatures of this transition as well, but the effects are smeared because this shot was taken in close proximity to the triple point. By contrast,  $\Delta P$  is zero in the dielectric phase. This phase is described as dielectric rather than paraelectric because at high temperatures, there are no electric dipoles created by the magnetic order, leaving just the background dielectric behavior of the atomic orbitals in  $(\text{NH}_4)_2[\text{FeCl}_5 \cdot (\text{H}_2\text{O})]$ .

Figure 2c,d display the magneto-electric current,  $I = dP/dt$ , as a function of applied field. Sharp peaks in the magneto-electric current denote the exact position of each transition. The fact



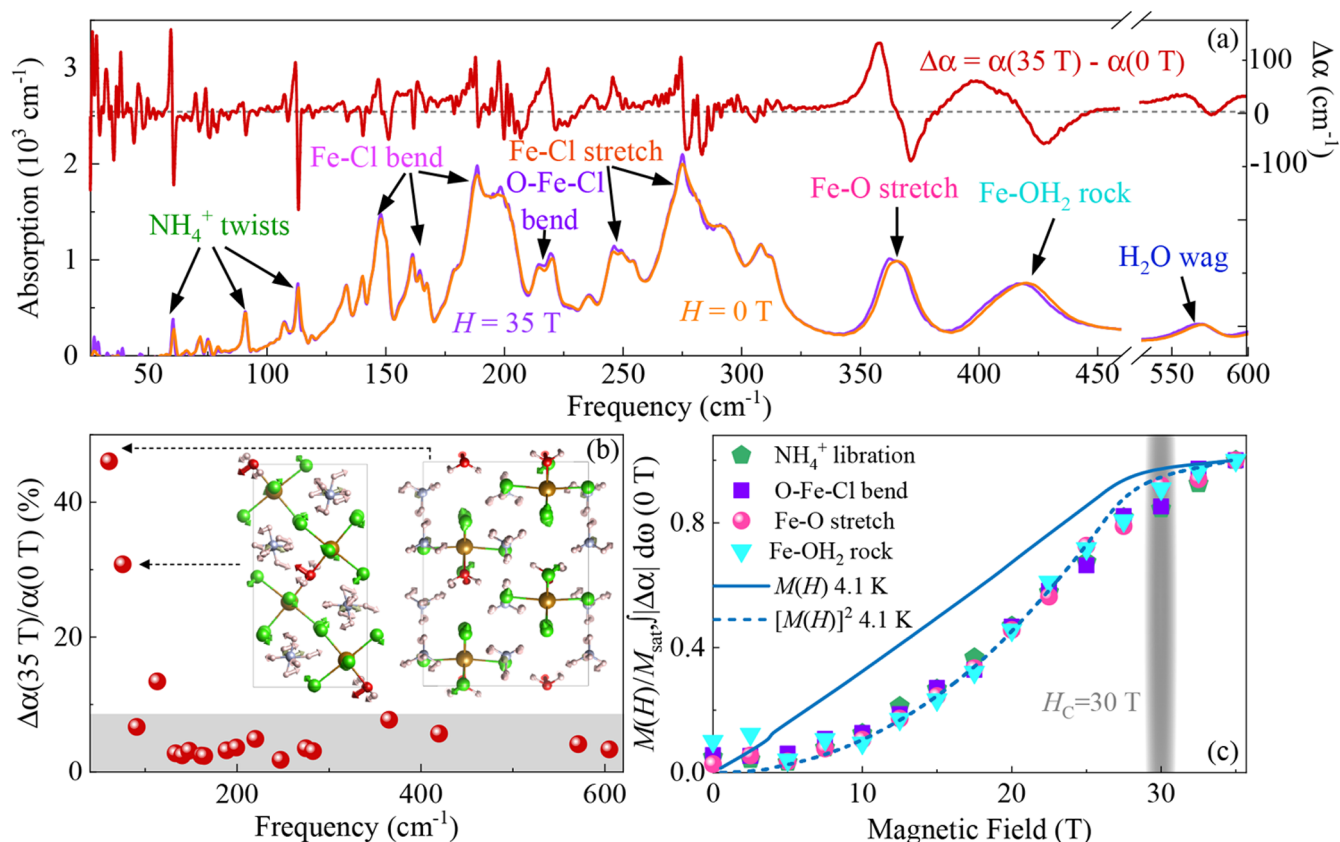


**Figure 3.** (a) Absorption spectrum of  $(\text{NH}_4)_2[\text{FeCl}_5(\text{H}_2\text{O})]$  at 0 and 35 T focusing on the low-frequency regime along with the full field absorption difference spectrum,  $\Delta\alpha = \alpha(35\text{ T}) - \alpha(0\text{ T})$ . Data are taken at 4.2 K. All vibrational modes in this region are magneto-active, whereas those above 600  $\text{cm}^{-1}$  are completely rigid. (b) Analysis of the percent changes in low-frequency phonons across the magnetic phase transition, along with calculated displacement patterns of two characteristic phonons involving H<sub>2</sub>O ligand motion and  $\text{NH}_4^+$  counterion libration. (c) Comparison of the integrated area of the absorption difference spectra for several different magneto-active vibrations along with the low-temperature magnetization<sup>21</sup> and the square of magnetization. The critical field, where the spins are fully saturated, is indicated in gray.

that peaks in the magnetoelectric current coincide with magnetically driven transitions<sup>20,21</sup> demonstrates that  $(\text{NH}_4)_2[\text{FeCl}_5(\text{H}_2\text{O})]$  is a high field multiferroic. As a reminder, the correspondence of high field electric polarization and magnetic transitions is evidence of magnetoelectric coupling, while the fact that poling controls the sign of the electric polarization provides evidence for ferroelectricity and thus multiferroic behavior. We extract a magnetoelectric coupling constant from our data as  $\alpha_{\text{me}} = (\partial P / \partial H)_T$ . We find that  $\alpha_{\text{me}}$  is 1.2 ps/m for the  $P\parallel c$ ,  $H\parallel c$  configuration between 5 and 25 T at 1.5 K—comparable with that in other multiferroics.

Within the  $p$ - $d$  hybridization mechanism,<sup>40,41</sup> the electric polarization induced by charge transfer from a metal ion with spin  $S$  to the ligand along vector  $\mathbf{e}$  is proportional to  $(\mathbf{e} \cdot \mathbf{S})S$ . We apply this result to the spin arrangement above the spin-flop transition assuming that  $\mathbf{e}$  points between the coupled  $\text{Fe}^{3+}$  ions. Then, the predicted electric polarization for magnetic field applied along either the  $a$  or  $c$  axis is proportional to  $c \sin 2\theta$ , where  $\theta$  is the tilting angle of the spins from the  $c$  axis due to the magnetic field. Since  $\sin \theta \propto H$ , the induced polarization is predicted to increase linearly with field for small  $\theta$ .<sup>41</sup> For the field along both  $a$  and  $c$ , the electric polarization is indeed dominated by the  $c$  component. We would expect that the polarization along  $c$  reaches a maximum when  $\theta = \pi/4$  or when the magnetization equals about 70% of its saturation value, in rough agreement with our measure-

ments. Of course, superexchange in this system is not mediated by a single ligand or overlap of  $p$  and  $d$  orbitals. Instead, each magnetic coupling between  $\text{Fe}^{3+}$  ions is mediated by two intermolecular  $\text{O}\cdots\text{Cl}$  or  $\text{Cl}\cdots\text{Cl}$  linkages. Even so, the orbital hybridization model correctly predicts that the electric polarization in the spin-flop phase is a linear function of magnetic field in the  $c$  direction (Figure 2a), and that it reaches a maximum before decreasing again.<sup>41</sup> It also predicts that the response along  $a$  is zero above 5 T, which is also observed in our measurements (Supporting Information).

The crystal structure of  $(\text{NH}_4)_2[\text{FeCl}_5(\text{H}_2\text{O})]$  below the order-disorder transition has been challenging to resolve.<sup>38,42,43</sup> Even so, we can assess the possibility of monoclinic domain formation. Naturally, monoclinic domains should have the same  $c$  axis but different  $a$  and  $b$  axes. If present, they should appear as a distribution of polarization states with different polarizations, some of which would be along  $a$  and others along  $b$ . That we do not observe polarizations only along  $a$  and  $b$  suggests that we do not see such monoclinic domains. If there were a distribution of monoclinic domains, there would be a distribution of polarizations along both the  $a$  and  $b$  axes.

Bringing these polarization results together with prior magnetization work,<sup>20,21</sup> we develop a magnetic field-temperature ( $H$ - $T$ ) phase diagram that summarizes the behavior of both charge and spin as well as the interaction between electric polarization and the spin arrangement (Figure

2e). The fact that the polarization flops from  $a$  to  $c$  across the cycloidal  $\rightarrow$  quasicollinear magnetic transition at 5 T is an excellent demonstration of how the charge and spin channels interact in the low field regime. As expected, the 5 T transition is observed in both the  $P||c$ ,  $H||c$  and  $P||a$ ,  $H||c$  data sets; the 1.5 T transition ( $P||a' \rightarrow P||a''$ ) is only detected when  $P||a$ .<sup>39</sup> The high field behavior of  $(\text{NH}_4)_2[\text{FeCl}_5 \cdot (\text{H}_2\text{O})]$  provides an even more foundational demonstration of type II multiferroicity and magnetoelectric coupling. Polarization trends are not correlated with the 30 T magnetic saturation transition as one might naively expect. Instead,  $\Delta P$  plunges to zero across the magnetic reorientation transition near 27 T—evidence that the microscopic spin configuration has changed in a fundamental manner—despite the fact that the magnetic moment itself continues to grow. The fact that  $\Delta P$  goes to zero at the quasi-collinear to collinear-sinusoidal spin transition reveals that inversion symmetry is restored due to the development of a collinear state. Here, we can equate  $\Delta P$  with  $P$  because  $P = 0$  outside the inversion symmetry-breaking magnetic phases. Overall, very similar phase boundaries are identified by both steady<sup>20</sup> and pulsed field work. These results along with low field neutron diffraction work<sup>24,32</sup> suggest that all of the magnetic states above 27 T (including the fully saturated state) are likely to be collinear. In other words, the  $K_2 = (0\ 0\ 0.25)$  phase, which is the commensurate distorted cycloid phase, does not persist above 5 T. We also see that while inverse Dzyaloshinskii-Moriya and  $p$ - $d$  hybridization models account for magnetoelectric coupling at zero and low fields, respectively,  $(\text{NH}_4)_2[\text{FeCl}_5 \cdot (\text{H}_2\text{O})]$  maintains an orbital hybridization mechanism at the highest fields.

**Magneto-Infrared Response of Multiferroic  $(\text{NH}_4)_2[\text{FeCl}_5 \cdot (\text{H}_2\text{O})]$ .** *Infrared Spectroscopy and Vibrational Mode Assignments.*  $(\text{NH}_4)_2[\text{FeCl}_5 \cdot (\text{H}_2\text{O})]$  is well-studied in the infrared, although previous investigations focus primarily on vibrational motions of water-coordinated aquo complexes en masse and how the pattern varies with counterion substitution ( $\text{K}^+$ ,  $\text{Rb}^+$ ,  $\text{NH}_4^+$ ).<sup>44–46</sup> For the most part, prior efforts address the behavior of the fundamental excitations of the lattice above  $350\text{ cm}^{-1}$ .<sup>43–46</sup> Our interests are different and instead concentrate on the development of magnetoelectricity and the behavior of the lattice across the sequence of temperature- and field-driven transitions. Furthermore, we focus primarily on the low-frequency vibrational modes (Figure 3a). The Fe–Cl stretch at  $276\text{ cm}^{-1}$ , the Fe–O stretch at  $365\text{ cm}^{-1}$ , and the Fe–OH<sub>2</sub> stretch at  $420\text{ cm}^{-1}$  are of particular interest in this work. They are assigned based upon our lattice dynamics calculations and a careful comparison with chemically similar materials. We first assign localized excitations and then those that are more collective in nature. There are several important low-frequency twisting, torsional, and wagging motions of  $\text{NH}_4^+$  and  $\text{H}_2\text{O}$  as well. The  $\text{NH}_4^+$ -related features are located mostly below  $200\text{ cm}^{-1}$ , and a prominent  $\text{H}_2\text{O}$  libration is near  $450\text{ cm}^{-1}$ .<sup>43–45</sup> A full set of assignments as well as a complete discussion of temperature trends across the 79 K order–disorder and 6.9 K ferroelectric transitions is available in the Supporting Information.

*Spin-Phonon Coupling Across the Magnetic Saturation Transition.* Figure 3a summarizes the magneto-infrared response of  $(\text{NH}_4)_2[\text{FeCl}_5 \cdot (\text{H}_2\text{O})]$  across the 30 T transition to the fully saturated spin state. In addition to absolute absorption at zero and 35 T, we also show a full field absorption difference curve  $\Delta\alpha = \alpha(35\text{ T}) - \alpha(0\text{ T})$ , which serves to emphasize small spectral changes under a magnetic

field. Remarkably, and without exception, all lattice distortions below  $600\text{ cm}^{-1}$  are sensitive to applied magnetic field, whereas those above this frequency are completely rigid. This behavior is entirely different from that of the copper halide coordination polymers like  $\text{Cu}(\text{pyz})(\text{NO}_3)_2$  or  $[\text{Cu}(\text{pyz})_2(2\text{-HOpy})_2](\text{PF}_6)_2$  where only one or two vibrational modes are sensitive to the magnetically driven phase transition.<sup>47–49</sup> Normalizing the absorption difference data as  $\Delta\alpha(35\text{ T})/\alpha(0\text{ T})$  allows us to evaluate the magnitude of these effects. The majority of local lattice distortions change by less than 10% in a 35 T magnetic field, although several of the lowest frequency modes reveal much larger field-induced modifications—up to 46% (Figure 3b). These motions are highly collective in nature and involve both  $\text{H}_2\text{O}$  ligand motion and  $\text{NH}_4^+$  counterion librations.<sup>43–45</sup> Displacement patterns for two characteristic distortions are included in the inset.

In order to quantify these effects, we integrate the absolute value of the absorption difference over an appropriate frequency window  $\int |\Delta\alpha| d\omega$  and plot these results as a function of magnetic field. In this way, we can reveal how specific local lattice distortions correlate with the development of the magnetic state. Figure 3c displays the integrated absorption differences of several important vibrational modes along with the low temperature magnetization<sup>21</sup> and the square of the magnetization.  $\int |\Delta\alpha| d\omega$  starts small, rises, and reaches a plateau as the magnetization saturates. All modes track  $[M(H)]^2$  remarkably well, demonstrating that the local lattice distortions are sensitive to the microscopic nature of the spin state.<sup>47,48,50</sup> That said, it is the magnetic saturation transition at 30 T, not the myriad of weaker spin reorientations evident in the  $H$ – $T$  phase diagram<sup>21</sup> or the loss of the inversion center above 27 T, that governs spin-phonon coupling in  $(\text{NH}_4)_2[\text{FeCl}_5 \cdot (\text{H}_2\text{O})]$ .

We evaluate spin-phonon coupling across the magnetically driven phase transition at 30 T as  $\omega = \omega_0 + \lambda \langle S_i S_j \rangle$  where  $\omega$  and  $\omega_0$  are the perturbed and unperturbed phonon frequencies,  $\lambda$  is the mode-dependent spin-phonon coupling constant, and  $\langle S_i S_j \rangle$  is the nearest-neighbor spin–spin correlation function. The magnitude of  $\lambda$  quantifies how the magnetic exchange interaction  $J$  is modulated by the various phonon displacements.<sup>51,52</sup> Using the limiting low temperature value of  $\langle S_i S_j \rangle = S^2 = (5/2)^2 = 6.25$ , we calculate  $\lambda$  for several important distortions including the Fe–O stretch, the Fe–OH<sub>2</sub> rocking mode, and the  $\text{NH}_4^+$  twist near  $60\text{ cm}^{-1}$ . These values are summarized in Table 1. Table S2 in the Supporting Information provides details of these calculations. The coupling constants for the two Fe-containing modes are on the order of  $-0.2$  and  $-0.3\text{ cm}^{-1}$ , and that of the ammonium libration is an order of magnitude lower. These values are significantly smaller than the coupling constants of other molecule-based materials such as the low-dimensional copper halides across their magnetic saturation transitions.<sup>52</sup> We attribute the difference to (i) through-space hydrogen- and halogen-bond exchange pathways in  $(\text{NH}_4)_2[\text{FeCl}_5 \cdot (\text{H}_2\text{O})]$  as compared with superexchange pathways created by metal–ligand–metal linkages in low-dimensional quantum magnets and (ii) the value of the spin ( $S = 5/2$  for  $\text{Fe}^{3+}$  vs  $1/2$  for  $\text{Cu}^{2+}$ ) which determines the size of the spin–spin correlation function.

**Local Lattice Distortions in the Ferroelectric State.** In order to uncover local lattice distortions across the ferroelectric transition, we examined the infrared response of  $(\text{NH}_4)_2[\text{FeCl}_5 \cdot (\text{H}_2\text{O})]$  as a function of temperature with

**Table 1. Summary of the Coupling Processes in  $(\text{NH}_4)_2[\text{FeCl}_5(\text{H}_2\text{O})]$  along with the Overall Size of Each Effect and Mechanisms<sup>a</sup>**

type of coupling	overall size	coupling mechanism
magnetoelectric coupling	$19 \mu\text{C}/\text{m}^2$ (24 T, $P \parallel c$ , $H \parallel c$ , 1.5 K) $\alpha_{\text{me}} = 1.2 \text{ ps/m}$ (5 – 25 T)	spin-charge interaction $\alpha_{\text{me}} = (\partial P / \partial H)_T$ $\approx (\Delta P / \Delta H)_T$
spin–lattice interaction	$\lambda = -0.21$ for Fe–O stretch $\lambda = -0.33$ for Fe–OH <sub>2</sub> rocking $\lambda = -0.06$ for $\text{NH}_4^+$ twist	spin-phonon coupling $\omega = \omega_0 + \lambda \langle S_i \cdot S_j \rangle$

<sup>a</sup>Here,  $\alpha_{\text{me}}$  and  $\lambda$  are the magnetoelectric and spin-phonon coupling constants, respectively.

special attention to spectral changes near  $T_{\text{FE}} = 6.9$  K. Unfortunately, there are surprisingly strong thermal contraction effects—even at low temperature—which obscure any spectral changes across the ferroelectric transition. This makes the overall results of such an analysis inconclusive (Figure S3). Since large thermal contraction effects preclude a straightforward identification of the polar modes, we turn to high field spectroscopy. As a reminder, the ferroelectric transition is triggered by a magnetic transition in a type II multiferroic. Thus, lattice distortions due to ferroelectricity in  $(\text{NH}_4)_2[\text{FeCl}_5(\text{H}_2\text{O})]$  can (in principle) be revealed through an analysis of spectral changes across the field-driven ferroelectric  $\leftrightarrow$  dielectric transition. Magneto-infrared changes are significantly smaller here but uncontaminated by thermal contraction (Figure S4). Moreover, spectral changes thus obtained ignore certain differences in magnetic state and are at the limit of our sensitivity. It is, however, still possible to carry out an analysis. We find a number of features below  $300 \text{ cm}^{-1}$  that are sensitive to the development of ferroelectricity. These are primarily ammonium counterion twisting modes but also include small contributions from the Cl–Fe–Cl bend.<sup>38,53–56</sup> This finding is consistent with recent spin density calculations predicting that through-space hydrogen- and halogen-bonding interactions depend upon the magnetic state.<sup>21</sup> A full analysis is presented in the Supporting Information (Figures S3 and S4).

## SUMMARY AND OUTLOOK

We combine high field electric polarization, magneto-infrared spectroscopy, and lattice dynamics calculations with prior magnetization to explore the properties of  $(\text{NH}_4)_2[\text{FeCl}_5(\text{H}_2\text{O})]$ . This molecular multiferroic is held together entirely by intermolecular hydrogen and halogen bonds and, as a result of the overall low energy scales, is extraordinarily sensitive to external stimuli. Electric polarization grows linearly with increasing field, reaching a maximum near 24 T, and plunges to zero as the inversion center is lost near 27 T—consistent with expectations for a type II multiferroic. We extract a magnetoelectric coupling constant on the order of 1.2 ps/m for the  $P \parallel c$ ,  $H \parallel c$  configuration between 5 and 25 T at 1.5 K. This value of  $\alpha_{\text{me}}$  is comparable with what is found in other multiferroics. We also analyze the electric polarization and magnetoelectric current in terms of predictions for the  $p$ – $d$  hybridization mechanism and show that the coupling between metal ions by two different ligand pathways produces an

electric polarization that remains a linear function of the magnetic field up to nearly the point when the magnetization reaches 70% of its saturation value—consistent with an orbital hybridization mechanism. Combining these findings with prior magnetization work deepens the overall understanding of the competing states of matter in the magnetic field–temperature phase diagram. The fundamental excitations of the lattice are well integrated in this system. Magneto-infrared spectroscopy reveals that all of the vibrational modes below  $600 \text{ cm}^{-1}$  are sensitive to the field-induced transition to the fully saturated magnetic state. This is in striking contrast to many other molecule-based materials in which only a few local lattice distortions aid in the development of the fully saturated spin state. We analyze these findings in terms of spin-phonon coupling across the magnetically driven transition at 30 T and extract coupling constants for the Fe–O stretch and Fe–OH<sub>2</sub> rocking modes on the order of  $-0.2$  to  $-0.3 \text{ cm}^{-1}$ . That of the  $\text{NH}_4^+$  twist is an order of magnitude smaller. These distortions modify intermolecular hydrogen- and halogen-bonding pathways and, as a result, the superexchange interactions. We also employ changes in the magneto-infrared response to reveal distortions of the ammonium counterions across the ferroelectric transition. These effects are extremely subtle and involve  $\text{NH}_4^+$  librations. The coexistence of charge-spin–lattice mixing processes in  $(\text{NH}_4)_2[\text{FeCl}_5(\text{H}_2\text{O})]$  suggests that other external stimuli such as pressure or strain will be useful for modulating properties as well.

## METHODS

**Crystal Growth and Sample Preparation.** Large  $(\text{NH}_4)_2[\text{FeCl}_5(\text{H}_2\text{O})]$  single crystals were obtained using solution techniques with HCl,  $\text{FeCl}_3$ , and  $\text{NH}_4\text{Cl}$  as starting materials, similar to the method reported previously.<sup>20</sup> The saturated solution was kept at  $38^\circ\text{C}$  in an environment chamber to allow slow evaporation. The crystals are sensitive to air, so they were stored in a drybox. Crystal orientation was determined using the well-developed flat surfaces:  $[1\ 0\ 0]$ ,  $[2\ 1\ 0]$ ,  $[1\ 0\ 1]$ , and  $[0\ 1\ 1]$ . Surfaces were polished to reveal specific faces for polarization measurements. Capacitor plates were attached with Ag paint, and vacuum grease was used to mount the crystals onto the probe tip. For the infrared work, the sample was mixed with paraffin or KBr for far and middle infrared spectroscopy, respectively. This allows control of optical density. Where necessary, the samples were mounted on pinholes with rubber cement.

**Polarization Measurements.** Pulsed-field polarization was measured in two different ways: (i) by poling the sample while cooling in a  $33 \text{ kV/m}$  electric field (applied voltage = 100 V, sample thickness = 3 mm) from above  $T_{\text{N}}$  to the final measurement temperature and then removing the electric field before measuring  $P(H)$  and (ii) by poling the sample as above and then leaving the electric field on while measuring  $P(H)$ . The first method proves that  $(\text{NH}_4)_2[\text{FeCl}_5(\text{H}_2\text{O})]$  is a ferroelectric since the electric polarization remains even after the electric field is removed. The data obtained from the second method yield a larger electric polarization, making it easier to identify each phase transition but otherwise show the same phase. We found similar results using both protocols. We can control the sign of the electric polarization by the direction of the poling field. The magnetoelectric current was measured by recording the change in surface charge on parallel capacitor plates applied with silver paint to the crystalline surface, using a SR570 current to voltage amplifier during a millisecond magnetic field pulse.<sup>57</sup> We integrated the measured magnetoelectric current with time to obtain the change in polarization  $\Delta P(H)$ . In order to remove any background signatures, we subtracted the 10 K polarization curve (which is well above the ferroelectric ordering temperature) from the low-temperature curves.

**Infrared Spectroscopy.** We employed a series of Fourier transform infrared spectrometers ( $20$ – $5000 \text{ cm}^{-1}$ ,  $2 \text{ cm}^{-1}$  resolution)



to measure the infrared vibrational response of  $(\text{NH}_4)_2[\text{FeCl}_5 \cdot (\text{H}_2\text{O})]$ . Absorption was calculated as  $\alpha(\omega) = -\frac{1}{hd} \ln[\mathcal{T}(\omega)]$  where  $h$  is the concentration,  $d$  is the thickness, and  $\mathcal{T}(\omega)$  is the measured transmittance. An open flow helium cryostat (4.2–300 K) provided temperature control. Magneto-infrared spectroscopy was performed at the National High Magnetic Field Laboratory in Tallahassee, Florida using a 35 T resistive magnet. In order to emphasize small spectral changes with the magnetic field, we calculate absorption differences as  $\Delta\alpha = \alpha(\omega, H) - \alpha(\omega, H = 0 \text{ T})$ . We quantify these results by integrating the absorption difference over an appropriate frequency window:  $\int |\Delta\alpha| d\omega$ . The integration limits vary for each phonon.

**Theoretical Approach.** First-principles calculations were performed using DFT within the local density approximation LDA + U method as implemented in the Vienna ab initio simulation package (VASP 5.4.1).<sup>58–60</sup> The Dudarev implementation<sup>61</sup> with on-site Coulomb interaction  $U = 2.0$  eV was used to treat the localized 3d electron states in Fe. Our value for  $U$  is chosen to bring spin propagation vector  $\mathbf{K}$  closest to the experimental value of  $\mathbf{K} = (0, 0, 0.23)$ .<sup>21,32,42</sup> The projector augmented wave (PAW) potentials<sup>62,63</sup> explicitly include eight valence electrons for Fe ( $3d^7 4s^1$ ), five for N ( $2s^2 2p^3$ ), one for H ( $1s^1$ ), seven for Cl ( $3s^2 3p^5$ ), and six for O ( $2s^2 2p^4$ ). The experimental crystal structure at 2 K was used as the initial structure<sup>28</sup> and then optimized for both lattice parameters and atomic positions with collinear-antiferromagnetic spin ordering. A plane-wave basis set with a cutoff energy of 500 eV was used. The k-point sampling used the Monkhorst–Pack<sup>64</sup> scheme and employed  $4 \times 6 \times 8$  mesh for structure optimization and IR calculation of the  $(\text{NH}_4)_2[\text{FeCl}_5 \cdot (\text{H}_2\text{O})]$  unit cell. The atomic positions were optimized until the interatomic forces were smaller than 1 meV/Å. The DFPT linear response calculation and Born effective charges are used to obtain infrared intensities.<sup>65–72</sup>

## ■ ASSOCIATED CONTENT

### SI Supporting Information

The Supporting Information is available free of charge at <https://pubs.acs.org/doi/10.1021/acs.inorgchem.1c03311>.

Magnetic field-induced polarization in other  $P/H$  configurations, tabulated vibrational mode assignments, a discussion of spectral changes across the order–disorder transition, and analyses of local lattice distortions across the ferroelectric transition (PDF)

## ■ AUTHOR INFORMATION

### Corresponding Author

Janice L. Musfeldt – Department of Chemistry and Department of Physics, University of Tennessee, Knoxville, Tennessee 37996, United States; [orcid.org/0000-0002-6241-823X](https://orcid.org/0000-0002-6241-823X); Email: [musfeldt@utk.edu](mailto:musfeldt@utk.edu)

### Authors

Kendall D. Hughey – Department of Chemistry, University of Tennessee, Knoxville, Tennessee 37996, United States; [orcid.org/0000-0002-8501-5425](https://orcid.org/0000-0002-8501-5425)

Minseong Lee – National High Magnetic Field Laboratory, Los Alamos National Laboratory, Los Alamos, New Mexico 87545, United States

Jisoo Nam – School of Energy and Chemical Engineering, Ulsan National Institute of Science and Technology, Ulsan 44919, Korea

Amanda J. Clune – Department of Chemistry, University of Tennessee, Knoxville, Tennessee 37996, United States; [orcid.org/0000-0001-8618-1700](https://orcid.org/0000-0001-8618-1700)

Kenneth R. O'Neal – Department of Chemistry, University of Tennessee, Knoxville, Tennessee 37996, United States; [orcid.org/0000-0001-9149-1957](https://orcid.org/0000-0001-9149-1957)

Wei Tian – Neutron Scattering Division, Oak Ridge National Laboratory, Oak Ridge, Tennessee 37831, United States

Randy S. Fishman – Materials Science and Technology Division, Oak Ridge National Laboratory, Oak Ridge, Tennessee 37831, United States

Mykhaylo Ozerov – National High Magnetic Field Laboratory, Florida State University, Florida 32310, United States; [orcid.org/0000-0002-5470-1158](https://orcid.org/0000-0002-5470-1158)

JunHee Lee – School of Energy and Chemical Engineering, Ulsan National Institute of Science and Technology, Ulsan 44919, Korea; [orcid.org/0000-0001-5121-244X](https://orcid.org/0000-0001-5121-244X)

Vivien S. Zapf – National High Magnetic Field Laboratory, Los Alamos National Laboratory, Los Alamos, New Mexico 87545, United States; [orcid.org/0000-0002-8375-4515](https://orcid.org/0000-0002-8375-4515)

Complete contact information is available at:

<https://pubs.acs.org/10.1021/acs.inorgchem.1c03311>

## Notes

The authors declare no competing financial interest.

Data are available from the corresponding author upon reasonable request.

## ■ ACKNOWLEDGMENTS

Research at Tennessee is supported by the National Science Foundation (DMR-1707846). A portion of this work was performed at the National High Magnetic Field Laboratory, which is supported by National Science Foundation Cooperative Agreement No. DMR-1644779 and the State of Florida. V.S.Z., W.T., and R.S.F. acknowledge funding from the U.S. Department of Energy, Office of Science, Basic Energy Sciences, Materials Sciences and Engineering Division, Condensed Matter Experiment and Theory Programs. J.H.L. and J.N. at UNIST were supported by Basic Research Laboratory (NRF2017R1A4A1015323), Midcareer Researcher (2020R1A2C2103126), and Creative Materials Discovery (2017M3D1A1040828) programs through the National Research Foundation of Korea, the MOTIE (Ministry of Trade, Industry and Energy; No. 10080657), and KRSC (Korea Semiconductor Research Consortium) support program. We thank Mark Turnbull for useful conversations.

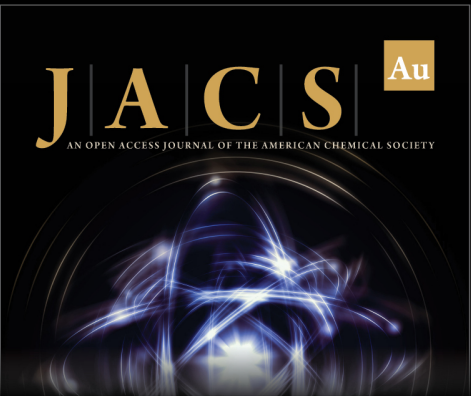
## ■ REFERENCES

- (1) Khomskii, D. Classifying multiferroics: mechanisms and effects. *Physics (College Park, Md.)* **2009**, *2*, 20.
- (2) Vecchini, C.; Chapon, L. C.; Brown, P. J.; Chatterji, T.; Park, S.; Cheong, S.-W.; Radaelli, P. G. Commensurate magnetic structures of  $\text{RMn}_2\text{O}_5$  ( $R = \text{Y, Ho, Bi}$ ) determined by single-crystal neutron diffraction. *Phys. Rev. B* **2008**, *77*, 134424.
- (3) Cheong, S.-W.; Mostovoy, M. Multiferroics: a magnetic twist for ferroelectricity. *Nat. Mater.* **2007**, *6*, 13–20.
- (4) Tokura, Y.; Seki, S.; Nagaosa, N. Multiferroics of spin origin. *Rep. Prog. Phys.* **2014**, *77*, 076501.
- (5) Jain, P.; Ramachandran, V.; Clark, R. J.; Zhou, H. D.; Toby, B. H.; Dalal, N. S.; Kroto, H. W.; Cheetham, A. K. Multiferroic behavior associated with an order-disorder hydrogen bonding transition in metal-organic frameworks (MOFs) with the perovskite  $\text{ABX}_3$  architecture. *J. Am. Chem. Soc.* **2009**, *131*, 13625–13627.
- (6) Jain, P.; Stroppa, A.; Nabok, D.; Marino, A.; Rubano, A.; Paparo, D.; Matsubara, M.; Nakotte, H.; Fiebig, M.; Picozzi, S.; Choi, E. S.; Cheetham, A. K.; Draxl, C.; Dalal, N. S.; Zapf, V. S. Switchable electric polarization and ferroelectric domains in a metal-organic-framework. *npj Quantum Mater.* **2016**, *1*, 16012.
- (7) Gomez-Aguirre, L. C.; Pato-Doldan, B.; Mira, J.; Castro-Garcia, S.; Senaris-Rodriguez, M. A.; Sanchez-Andujar, M.; Singleton, J.; Zapf,


- V. S. Magnetic ordering-induced multiferroic behavior in  $[\text{CH}_3\text{NH}_3]\text{[Co(HCOO)}_3\text{]}$  metal-organic framework. *J. Am. Chem. Soc.* **2016**, *138*, 1122–1125.
- (8) Pardo, E.; Train, C.; Liu, H.; Chamoireau, L. M.; Dkhil, B.; Boubekeur, K.; Lloret, F.; Nakatani, K.; Tokoro, H.; Ohkoshi, S. I.; Verdaguer, M. Multiferroics by rational design: implementing ferroelectricity in molecule-based magnets. *Angew. Chemie - Int. Ed.* **2012**, *51*, 8356–8360.
- (9) Cai, H. L.; Zhang, Y.; Fu, D. W.; Zhang, W.; Liu, T.; Yoshikawa, H.; Awaga, K.; Xiong, R. G. Above-room-temperature magnetodielectric coupling in a possible molecule-based multiferroic: triethylmethylammonium tetrabromoferrate(III). *J. Am. Chem. Soc.* **2012**, *134*, 18487–18490.
- (10) Cañadillas-Delgado, L.; Fabelo, O.; Rodríguez-Velamazán, J. A.; Lemée-Cailleau, M. H.; Mason, S. A.; Pardo, E.; Lloret, F.; Zhao, J. P.; Bu, X. H.; Simonet, V.; Colin, C. V.; Rodríguez-Carvajal, J. The role of order-disorder transitions in the quest for molecular multiferroics: structural and magnetic neutron studies of a mixed valence iron(II)-iron(III) formate framework. *J. Am. Chem. Soc.* **2012**, *134*, 19772–19781.
- (11) Bosch-Serrano, C.; Clemente-Juan, J. M.; Coronado, E.; Gaita-Ariño, A.; Pali, A.; Tsukerblat, B. Molecular analog of multiferroics: electric and magnetic field effects in many-electron mixed-valence dimers. *Phys. Rev. B* **2012**, *86*, 024432.
- (12) Wu, S. Y. Applications of Raman microscopy for spin-phonon coupling and magnon excitation study in nanocrystals. *Curr. Microsc. Contrib. to Adv. Sci. Technol.* **2012**, *3*, 1036–1043.
- (13) Zapf, V. S.; Kenzelmann, M.; Wolff-Fabris, F.; Balakirev, F.; Chen, Y. Magnetically induced electric polarization in an organometallic magnet. *Phys. Rev. B* **2010**, *82*, No. 060402(R).
- (14) Stroppa, A.; Barone, P.; Jain, P.; Perez-Mato, J. M.; Picozzi, S. Hybrid improper ferroelectricity in a multiferroic and magnetoelectric metal-organic framework. *Adv. Mater.* **2013**, *25*, 2284–2290.
- (15) Clune, A.; Hughey, K.; Lee, C.; Abhyankar, N.; Ding, X.; Dalal, N.; Whangbo, M.-H.; Singleton, J.; Musfeldt, J. Magnetic field-temperature phase diagram of multiferroic  $[(\text{CH}_3)_2\text{NH}_2]\text{Mn}(\text{HCOO})_3$ . *Phys. Rev. B* **2017**, *96*, 104424.
- (16) Lancaster, T.; et al. Controlling magnetic order and quantum disorder in molecule-based magnets. *Phys. Rev. Lett.* **2014**, *112*, 207201.
- (17) Brambleby, J.; Manson, J. L.; Goddard, P. A.; Stone, M. B.; Johnson, R. D.; Manuel, P.; Villa, J. A.; Brown, C. M.; Lu, H.; Chikara, S.; Zapf, V.; Lapidus, S. H.; Scatena, R.; Macchi, P.; Chen, Y.-s.; Wu, L.-C.; Singleton, J.; et al. Combining microscopic and macroscopic probes to untangle the single-ion anisotropy and exchange energies in an  $S = 1$  quantum antiferromagnet. *Phys. Rev. B* **2017**, *95*, 234435.
- (18) Lunkenheimer, P.; Müller, J.; Krohns, S.; Schrettle, F.; Loidl, A.; Hartmann, B.; Rommel, R.; De Souza, M.; Hotta, C.; Schlueter, J. A.; Lang, M. Multiferroicity in an organic charge-transfer salt that is suggestive of electric-dipole-driven magnetism. *Nat. Mater.* **2012**, *11*, 755–758.
- (19) Zapf, V. S.; Sengupta, P.; Batista, C. D.; Nasreen, F.; Wolff-Fabris, F.; Paduan-Filho, A. Magnetoelectric effects in an organometallic quantum magnet. *Phys. Rev. B* **2011**, *83*, No. 140405(R).
- (20) Ackermann, M.; Brüning, D.; Lorenz, T.; Becker, P.; Bohatý, L. Thermodynamic properties of the new multiferroic material  $(\text{NH}_4)_2[\text{FeCl}_5(\text{H}_2\text{O})]$ . *New J. Phys.* **2013**, *15*, 123001.
- (21) Clune, A. J.; Nam, J.; Lee, M.; Hughey, K. D.; Tian, W.; Fernandez-Baca, J. A.; Fishman, R. S.; Singleton, J.; Lee, J. H.; Musfeldt, J. L. Magnetic field-temperature phase diagram of multiferroic  $(\text{NH}_4)_2\text{FeCl}_5\cdot\text{H}_2\text{O}$ . *npj Quantum Mater.* **2019**, *4*, 44.
- (22) Tian, W.; Cao, H.; Wang, J.; Ye, F.; Matsuda, M.; Yan, J.-Q.; Liu, Y.; Garlea, V. O.; Agrawal, H. K.; Chakoumakos, B. C.; Sales, B. C.; Fishman, R. S.; Fernandez-Baca, J. A. Spin-lattice coupling mediated multiferroicity in  $(\text{ND}_4)_2\text{FeCl}_5\cdot\text{D}_2\text{O}$ . *Phys. Rev. B* **2016**, *94*, 214405.
- (23) Tian, W.; Cao, H. B.; Clune, A. J.; Hughey, K. D.; Hong, T.; Yan, J.-Q.; Agrawal, H. K.; Singleton, J.; Sales, B. C.; Fishman, R. S.; Musfeldt, J. L.; Fernandez-Baca, J. A. Electronic phase separation and magnetic-field-induced phenomena in molecular multiferroic  $(\text{ND}_4)_2\text{FeCl}_5\cdot\text{D}_2\text{O}$ . *Phys. Rev. B* **2018**, *98*, 054407.
- (24) Alberto Rodríguez-Velamazán, J.; Fabelo, O.; Millán, A.; Campo, J.; Johnson, R. D.; Chapon, L. Magnetically-induced ferroelectricity in the  $(\text{ND}_4)_2[\text{FeCl}_5(\text{D}_2\text{O})]$  molecular compound. *Sci. Rep.* **2015**, *5*, 14475.
- (25) Bai, X.; Fishman, R. S.; Sala, G.; Pajeroski, D. M.; Garlea, V. O.; Hong, T.; Lee, M.; Fernandez-Baca, J. A.; Cao, H.; Tian, W. Magnetic excitations of the hybrid multiferroic  $(\text{ND}_4)_2\text{FeCl}_5\cdot\text{D}_2\text{O}$ . *Phys. Rev. B* **2021**, *103*, 224411.
- (26) Cavallo, G.; Metrangolo, P.; Milani, R.; Pilati, T.; Priimagi, A.; Resnati, G.; Terraneo, G. The Halogen Bond. *Chem. Rev.* **2016**, *116*, 2478–2601.
- (27) McElearney, J. N.; Merchant, S. Nonisomorphic antiferromagnetic behavior of two isomorphic salts: low-temperature heat capacities and magnetic susceptibilities of  $(\text{NH}_4)_2\text{FeCl}_5\cdot\text{H}_2\text{O}$  and  $\text{K}_2\text{FeCl}_5\cdot\text{H}_2\text{O}$ . *Inorg. Chem.* **1978**, *17*, 1207–1215.
- (28) Figgis, B. N.; Raston, C. L.; Sharma, R. P.; White, A. H. Crystal structure of diammonium aquapentachloroferrate(III). *Aust. J. Chem.* **1978**, *31*, 2717–2720.
- (29) Campo, J.; Luzón, J.; Palacio, F.; McIntyre, G. J.; Millán, A.; Wildes, A. R. Understanding magnetic interactions in the series  $\text{A}_2\text{FeX}_5\cdot\text{H}_2\text{O}$  ( $\text{A}=\text{K}, \text{Rb}$ ;  $\text{X}=\text{Cl}, \text{Br}$ ). II. Inelastic neutron scattering and DFT studies. *Phys. Rev. B* **2008**, *78*, 054415.
- (30) Schultz, A. J.; Carlin, R. L. Single-crystal pulsed neutron diffraction structure of the antiferromagnet  $\text{K}_2[\text{FeCl}_5(\text{H}_2\text{O})]$  with and without applied pressure. *Acta Crystallogr. Sect. B* **1995**, *51*, 43–47.
- (31) Lee, M. Magnetic phase diagram of erythrosiderites. *arXiv* **2021**, arXiv:2103.08500v1.
- (32) Rodríguez-Velamazán, J. A.; Fabelo, O.; Campo, J.; Millán, Á.; Rodríguez-Carvajal, J.; Chapon, L. C. Magnetic-field-induced change of magnetoelectric coupling in the hybrid multiferroic  $(\text{ND}_4)_2[\text{FeCl}_5\cdot\text{D}_2\text{O}]$ . *Phys. Rev. B* **2017**, *95*, 174439.
- (33) Chen, S. W.; et al. Exchange interaction mediated ferroelectricity in multiferroic  $\text{MnTiO}_3$  with anisotropic orbital hybridization and hole delocalization. *Appl. Phys. Lett.* **2014**, *104*, 082104.
- (34) Yamasaki, Y.; Okuyama, D.; Nakamura, M.; Arima, T.-h.; Kawasaki, M.; Tokura, Y.; Kimura, T.; Wakabayashi, Y. Interfacial structure of Manganite superlattice. *J. Phys. Soc. Jpn.* **2011**, *80*, 073601.
- (35) Murakawa, H.; Onose, Y.; Miyahara, S.; Furukawa, N.; Tokura, Y. Ferroelectricity induced by spin-dependent metal-ligand hybridization in  $\text{Ba}_2\text{CoGe}_2\text{O}_7$ . *Phys. Rev. Lett.* **2010**, *105*, 137202.
- (36) Moskvina, A. S.; Drechsler, S. L. Microscopic mechanisms of spin-dependent electric polarization in 3d oxides. *Phys. Rev. B* **2008**, *78*, 024102.
- (37) Tang, Y. S.; et al. Metamagnetic transitions and magnetoelectricity in the spin-1 honeycomb antiferromagnet  $\text{Ni}_2\text{Mo}_3\text{O}_8$ . *Phys. Rev. B* **2021**, *103*, 014112.
- (38) Brüning, D.; Fröhlich, T.; Langenbach, M.; Leich, T.; Meven, M.; Becker, P.; Bohatý, L.; Grüninger, M.; Braden, M.; Lorenz, T. Magnetoelectric coupling in the mixed erythrosiderite  $[(\text{NH}_4)_{1-x}\text{K}_x]_2[\text{FeCl}_5(\text{H}_2\text{O})]$ . *Phys. Rev. B* **2020**, *102*, 054413.
- (39) In the  $P||a'$  phase, polarization lies within the  $ab$  plane and is oriented  $7^\circ$  off of the  $a$  axis. Above 1.5 T ( $H||c$ ) at low temperatures, polarization tilts to  $P||a'''$  and orients within the same plane but approximately  $5^\circ$  off of the  $a$  axis.
- (40) Jia, C.; Onoda, S.; Nagaosa, N.; Han, J. H. Microscopic theory of spin-polarization coupling in multiferroic transition metal oxides. *Phys. Rev. B* **2007**, *76*, 144424.
- (41) Li, S.; Fishman, R. S. Phase transitions of the ferroelectric  $(\text{ND}_4)_2\text{FeCl}_5\cdot\text{D}_2\text{O}$  under magnetic field. *Phys. Rev. B* **2021**, *104*, L060407.
- (42) Alberto Rodríguez-Velamazán, J.; Fabelo, O.; Millán, A.; Campo, J.; Johnson, R. D.; Chapon, L. Magnetically-induced ferroelectricity in the  $(\text{ND}_4)_2[\text{FeCl}_5(\text{D}_2\text{O})]$  molecular compound. *Sci. Rep.* **2015**, *5*, 14475.



- (43) Lacková, D.; Ondrejčovičová, I.; Koman, M. A new pathway of preparation and refined structure of  $(\text{NH}_4)_2[\text{FeCl}_5(\text{H}_2\text{O})]$ . *Acta Chim. Slovaca* **2013**, *6*, 129–132.
- (44) Adams, M.; Lock, P. J. A survey study of the vibrational spectra of some aquo-halogeno-complexes. *J. Chem. Soc. A Inorganic, Phys. Theor.* **1971**, 2801–2806.
- (45) Falk, M.; Huang, C.-H.; Knop, O. Infrared studies of water in crystalline hydrates:  $\text{K}_2\text{FeCl}_5 \cdot \text{H}_2\text{O}$  (erythrosiderite) and related aquopentachloroferrates(III). *Can. J. Chem.* **1975**, *53*, 51–57.
- (46) Sharma, S. K.; Pandya, D. K. Laser-Raman spectra of crystalline  $(\text{NH}_4)\text{FeCl}_5 \cdot \text{H}_2\text{O}$ ,  $\text{K}_2\text{FeCl}_5 \cdot \text{H}_2\text{O}$  and  $\text{K}_2\text{FeCl}_5 \cdot \text{D}_2\text{O}$ . *J. Inorg. Nucl. Chem.* **1974**, *36*, 1165–1166.
- (47) Günaydin-Şen, O.; Lee, C.; Tung, L. C.; Chen, P.; Turnbull, M. M.; Landee, C. P.; Wang, Y. J.; Whangbo, M.-H.; Musfeldt, J. L. Spin-lattice interactions through the quantum critical transition in  $\text{Cu}(\text{pyz})(\text{NO}_3)_2$ . *Phys. Rev. B* **2010**, *81*, 104307.
- (48) Al-Wahish, A.; O'Neal, K.; Lee, C.; Fan, S.; Hughey, K.; Yokosuk, M.; Clune, A.; Li, Z.; Schlueter, J.; Manson, J.; Whangbo, M.-H.; Musfeldt, J. Magnetic phase transitions and magnetoelastic coupling in  $S = 1/2$  Heisenberg antiferromagnets. *Phys. Rev. B* **2017**, *95*, 104437.
- (49) Hughey, K. D.; Clune, A. J.; Yokosuk, M. O.; Li, J.; Abhyankar, N.; Ding, X.; Dalal, N. D.; Xiang, H.; Smirnov, D.; Singleton, J.; Musfeldt, J. L. Structure-property relations in multiferroic  $[(\text{CH}_3)_2\text{NH}_2]\text{M}(\text{HCOO})_3$  ( $M = \text{Mn}, \text{Co}, \text{Ni}$ ). *Inorg. Chem.* **2018**, *57*, 11569–11577.
- (50) Granado, E.; García, A.; Sanjurjo, J. A.; Rettori, C.; Torriani, I.; Prado, F.; Sánchez, R. D.; Caneiro, A.; Oseroff, S. B. Magnetic ordering effects in the Raman spectra of  $\text{La}_{1-x}\text{Mn}_{1-x}\text{O}_3$ . *Phys. Rev. B* **1999**, *60*, 11879–11882.
- (51) Lee, J. H.; Rabe, K. M. Large spin-phonon coupling and magnetically induced phonon anisotropy in  $\text{SrMO}_3$  perovskites ( $M = \text{V}, \text{Cr}, \text{Mn}, \text{Fe}, \text{Co}$ ). *Phys. Rev. B* **2011**, *84*, 104440.
- (52) Hughey, K. D.; Harms, N. C.; O'Neal, K. R.; Clune, A. J.; Monroe, J. C.; Blockmon, A. L.; Landee, C. P.; Liu, Z.; Ozerov, M.; Musfeldt, J. L. Spin-lattice coupling across the magnetic quantum-phase transition in copper-containing coordination polymers. *Inorg. Chem.* **2020**, *59*, 2127–2135.
- (53) Ebisuzaki, Y. Raman spectra of  $\text{NH}_4\text{Cl}$  and  $\text{NH}_4\text{Br}$ : Dependence of the librational and the internal modes of the  $\text{NH}_4^+$  ion on volume and on nitrogen-halogen distance. *J. Chem. Phys.* **1974**, *61*, 3170–3180.
- (54) Suresh, G.; Ratheesh, R.; Pradip, T.; Manojkumar, K.; Nayar, V. U. Vibrational spectra of  $\text{NH}_4\text{Sm}(\text{SO}_4)_2 \cdot 4\text{H}_2\text{O}$  and  $\text{NH}_4\text{Ln}(\text{SO}_4)_2 \cdot 2\text{H}_2\text{O}$  [ $\text{Ln} = \text{Yb}, \text{Tm}$ ]. *J. Solid State Chem.* **1996**, *121*, 408–414.
- (55) Prager, M.; Grimm, H.; Natkaniec, I.; Nowak, D.; Unruh, T. The dimensionality of ammonium reorientation in  $(\text{NH}_4)_2\text{S}_2\text{O}_8$ : The view from neutron spectroscopy. *J. Phys.: Condens. Matter* **2008**, *20*, 125218.
- (56) Verdal, N.; Udovic, T. J.; Rush, J. J.; Stavila, V.; Wu, H.; Zhou, W.; Jenkins, T. Low-temperature tunneling and rotational dynamics of the ammonium cations in  $(\text{NH}_4)_2\text{B}_{12}\text{H}_{12}$ . *J. Chem. Phys.* **2011**, *135*, 094501.
- (57) Chikara, S.; Singleton, J.; Bowlan, J.; Yarotski, D. A.; Lee, N.; Choi, H. Y.; Choi, Y. J.; Zapf, V. S. Electric polarization observed in single crystals of multiferroic  $\text{Lu}_2\text{MnCoO}_6$ . *Phys. Rev. B* **2016**, *93*, No. 180405(R).
- (58) Kresse, G.; Hafner, J. Ab initio molecular dynamics for liquid metals. *Phys. Rev. B* **1993**, *47*, 558–561.
- (59) Kresse, G.; Furthmüller, J. Efficient iterative schemes for ab initio total-energy calculations using a plane-wave basis set. *Phys. Rev. B* **1996**, *54*, 11169–11186.
- (60) Perdew, J. P.; Burke, K.; Ernzerhof, M. Generalized gradient approximation made simple. *Phys. Rev. Lett.* **1996**, *77*, 3865–3868.
- (61) Dudarev, S. L.; Botton, G. A.; Savrasov, S. Y.; Humphreys, C. J.; Sutton, A. P. Electron-energy-loss spectra and the structural stability of nickel oxide: an LSDA+U study. *Phys. Rev. B* **1998**, *57*, 1505–1509.
- (62) Blöchl, P. E. Projector augmented-wave method. *Phys. Rev. B* **1994**, *50*, 17953–17979.
- (63) Kresse, G.; Joubert, D. From ultrasoft pseudopotentials to the projector augmented-wave method. *Phys. Rev. B* **1999**, *59*, 1758–1775.
- (64) Pack, J. D.; Monkhorst, H. J. Special points for Brillouin-zone integrations. *Phys. Rev. B* **1976**, *13*, 5188–5192.
- (65) Gonze, X.; Lee, C. Dynamical matrices, Born effective charges, dielectric permittivity tensors, and interatomic force constants from density-functional perturbation theory. *Phys. Rev. B* **1997**, *55*, 10355–10368.
- (66) Gonze, X. Perturbation expansion of variational principles at arbitrary order. *Phys. Rev. A* **1995**, *52*, 1086–1095.
- (67) Karhánek, D.; Bučko, T.; Hafner, J. A density-functional study of the adsorption of methane-thiol on the (111) surfaces of the Ni-group metals: II. Vibrational spectroscopy. *J. Phys.: Condens. Matter* **2010**, *22*, 265006.
- (68) Pick, R. M.; Cohen, M. H.; Martin, R. M. Microscopic theory of force constants in the adiabatic approximation. *Phys. Rev. B* **1970**, *1*, 910–920.
- (69) Wu, X.; Vanderbilt, D.; Hamann, D. R. Systematic treatment of displacements, strains, and electric fields in density-functional perturbation theory. *Phys. Rev. B* **2005**, *72*, 035105.
- (70) Gajdoš, M.; Hummer, K.; Kresse, G.; Furthmüller, J.; Bechstedt, F. Linear optical properties in the projector-augmented wave methodology. *Phys. Rev. B* **2006**, *73*, 045112.
- (71) Baroni, S.; de Gironcoli, S.; Dal Corso, A.; Giannozzi, P. Phonons and related crystal properties from density-functional perturbation theory. *Rev. Mod. Phys.* **2001**, *73*, 515–562.
- (72) Gonze, X. DFPT: Adiabatic density-functional perturbation theory. *Phys. Rev. A* **1995**, *52*, 1096–1114.



**JACS Au**  
AN OPEN ACCESS JOURNAL OF THE AMERICAN CHEMICAL SOCIETY



Editor-in-Chief  
**Prof. Christopher W. Jones**  
Georgia Institute of Technology, USA

**Open for Submissions**

pubs.acs.org/jacsau

ACS Publications  
Most Trusted. Most Cited. Most Read.